AGU100 ADVANCING EARTH AND SPACE SCIENCE

Water Resources Research

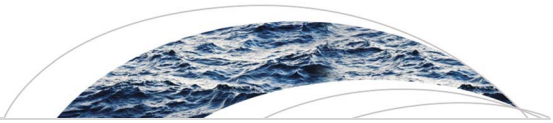

RESEARCH ARTICLE
10.1029/2018WR023194

Key Points:
- The methodology presented incorporates the observed spatial and temporal variability of rainfall in flood frequency analysis
- The proposed method accounts for the combined effect of antecedent soil moisture and rainfall intensity in flood frequency estimates
- With the proposed approach, there is no need to define synthetic design hyetographs for a given return period

Correspondence to:
L. Cea,
luis.cea@udc.es

Citation:
Cea, L., & Fraga, I. (2018). Incorporating antecedent moisture conditions and intraevent variability of rainfall on flood frequency analysis in poorly gauged basins. *Water Resources Research*, *54*, 8774–8791. https://doi.org/10.1029/2018WR023194

Received 24 APR 2018
Accepted 17 OCT 2018
Accepted article online 29 OCT 2018
Published online 8 NOV 2018

Incorporating Antecedent Moisture Conditions and Intraevent Variability of Rainfall on Flood Frequency Analysis in Poorly Gauged Basins

L. Cea[1] **and I. Fraga**[2]

[1]Environmental and Water Engineering Group, Department of Civil Engineering, Universidade da Coruña, Coruña, Spain, [2]CITIC, Universidade da Coruña, Coruña, Spain

Abstract Rainfall-runoff models are frequently used for the prediction of flood discharges from extreme rainfall data in poorly gauged basins. However, the conventional methods used to estimate the frequency of flood discharges from precipitation data do not incorporate a realistic representation of the spatial and temporal structure of rainfall at the study site nor of the antecedent soil moisture content. Temporally and spatially idealized rainfall patterns that do not represent properly the intraevent variability of rainfall are in general assumed. In this paper, we propose a methodology for flood frequency analysis based on the hydrological simulation of potentially hazardous real storm events. The aim of the proposed method is to incorporate the impact of the spatial and temporal intraevent variability of rainfall on flood discharge estimates without making strong assumptions about the spatial and temporal patterns of storms. It also includes a calibrated relation between the antecedent rainfall depth and the soil infiltration capacity, in order to consider the combined effect of antecedent soil moisture content and rainfall intensity. The flood frequency estimates obtained with the proposed methodology are compared to those estimated with a conventional method based on the definition of synthetic design hyetographs from local intensity-duration-frequency curves. The analysis is presented in two watersheds of 84 and 353 km^2 located in the NW of Spain. Results highlight the role of the antecedent soil moisture in flood frequency analysis and show that the conventional methodology tends to overestimate the flood discharges when compared to the proposed approach.

1. Introduction

Flood frequency analysis in poorly gauged basins (those that lack comprehensive streamflow data) relies either on empirical regional regression equations or on rainfall-runoff transformation modeling. Regional flood frequency analysis (RFFA) is commonly used when comprehensive streamflow data are available in catchments with similar hydrological and climatological characteristics as the study basin, even though some attempts have been done to develop these methods at the global scale (Smith et al., 2015). Although RFFA methods have proven to give reliable flood frequency estimates and are generally accepted in engineering practice, they remain a black box as they do not provide any knowledge about the physical processes that generate the floods at a specific basin (Dawdy et al., 2012). Conversely, methods based on physically based rainfall-runoff modeling can provide some understanding of the processes involved in the generation of floods, which might be relevant for engineering applications and for climate change studies (Dawdy et al., 2012). This paper deals with the application of rainfall-runoff transformation methods to flood frequency analysis, focusing on the incorporation of rainfall variability and antecedent soil moisture content at the event scale.

Conventional methods used in flood frequency estimation from precipitation data do not account properly for the spatial and temporal variability of rainfall during storm events. However, it has been shown in several studies that storm motion, which is one of the main causes of rainfall variability, has a relevant impact on flood peaks (De Lima & Singh, 2002; Liang & Melching, 2015; Mizumura & Ito, 2011; Sigaroodi & Chen, 2016). Standard procedures assume synthetic patterns to distribute the rainfall depth in time and space. The most common approach in engineering practice is to use the intensity-duration-frequency (IDF) curves evaluated at the site of interest from point rainfall historical data. A family of IDF curves contains some information about the interevent temporal structure of rainfall, but this information is incomplete and needs to be complemented with a synthetic hyetograph in order to define the temporal pattern of the design

hyetographs. One of the most common methods to do this is the Alternating Block Method (ABM), although there are others such as a triangular hyetograph, the Soil Conservation Service (SCS) storms (NRCS, 2007), or the HMR 52 storm (Hansen et al., 1982), which defines the spatial and temporal distribution of the probable maximum precipitation for a watershed. None of these hyetographs represents properly the temporal variability of real events, especially when several rainfall intensity peaks occur during a storm. However, even if temporal rainfall variability of real events shows substantial departure from idealized design storm hyetographs, the impacts of design storm assumptions, such as spatially uniform or idealized rainfall patterns, on flood risk estimates are still poorly understood (Wright et al., 2013, 2014a, 2014b). This omission contrasts with the well-known sensitivity of catchment response to rainfall distribution (Lobligeois et al., 2014; Niemi et al., 2016; Shen et al., 2012).

Regarding the spatial distribution of rainfall, the most common approach is to use either a single basin-averaged design hyetograph corresponding to a given return period in the whole catchment (assuming therefore a spatially homogeneous rainfall) or to use different design hyetographs (all of them corresponding to the same return period) at each subbasin of the hydrological model. In both cases, the peak rainfall intensity associated to a given return period occurs simultaneously over the whole catchment. This is an unrealistic assumption in medium and large catchments. In addition, it is unlikely that the rainfall depths registered at different locations during the same event have the same return period.

Areal reduction factors (ARFs), defined as the ratio between extreme area-averaged rainfall and extreme point rainfall, are commonly used to cope with this inconvenience (Asquith & Famiglietti, 2000; Bacchi & Ranzi, 1996; NERC, 1975; NSSP, 1961; Rodriguez-Iturbe & Mejía, 1974; Sivapalan & Blöschl, 1998; Vaes et al., 2005). If ARFs are known for the study catchment, effective rainfall depths can be computed by multiplying point depths by the ARF. However, the estimation of ARFs is difficult to generalize and extrapolate to other basins and storm conditions because they depend on the size, shape, and topography of the basin, on its geographic location and on the rainfall duration. In addition, several works have suggested that ARFs depend on return period (Sivapalan & Bloeschl 1998; Asquith & Famiglietti, 2000; Allen & DeGaetano 2005; Veneziano & Langousis 2005), which constrains even more their applicability. For these reasons, commonly used ARFs do not represent properly the real properties of extreme rainfall, and this might result in large errors in the estimation of flood discharges (Wright et al., 2014a).

In addition to the previous issues, when using a single design hyetograph for a given return period, it is difficult to establish the antecedent soil moisture content (AMC) that should be considered in the hydrological model to compute rainfall-runoff. This becomes especially important since the impact of antecedent rainfall on the soil infiltration capacity and thus on the generation of surface runoff is well known. The same flood discharge can originate from a high rainfall intensity falling over a moderately wet terrain or from a medium rainfall intensity falling over a saturated terrain. In most locations, soil moisture and extreme rainfall are cyclostationary and partially correlated random processes. Therefore, the statistical distribution of flooding depends on their joint distribution, which is in general unknown. However, conventional methods for the evaluation of design hyetographs do not account properly for the dependence between extreme rainfall and initial soil moisture conditions. Some authors have proposed methods to account for the joint variability between these two variables using long-term continuous hydrological simulations, including in some cases the generation of long-term synthetic series of weather variables (Blazkova & Beven, 2004; Brocca et al., 2011; Camici et al., 2011; Falter et al., 2015; Moretti & Montanari, 2008). All these works highlight the importance of considering the joint probability of occurrence of AMC and extreme rainfall in flood frequency analysis.

For the previous reasons, Wright et al. (2014a) suggest that, rather than updating methods that assume strong simplifications on the structure of rainfall, as ARF-based methods, research and practice should focus on flood estimation techniques that incorporate a realistic site-specific representation of the spatial and temporal structure of storm rainfall. Following this line, in this paper we analyze the impact of the spatial and temporal intra-event variability of rainfall on flood frequency analysis in poorly gauged basins using rainfall-runoff models. We propose a methodology based on the hydrological simulation of potentially hazardous real storm events. By poorly gauged basin, we refer to catchments with just a few measured discharge data over a limited period of time, sufficient to calibrate a hydrological model but insufficient to perform a statistical flood frequency analysis on streamflow data. The proposed method includes a

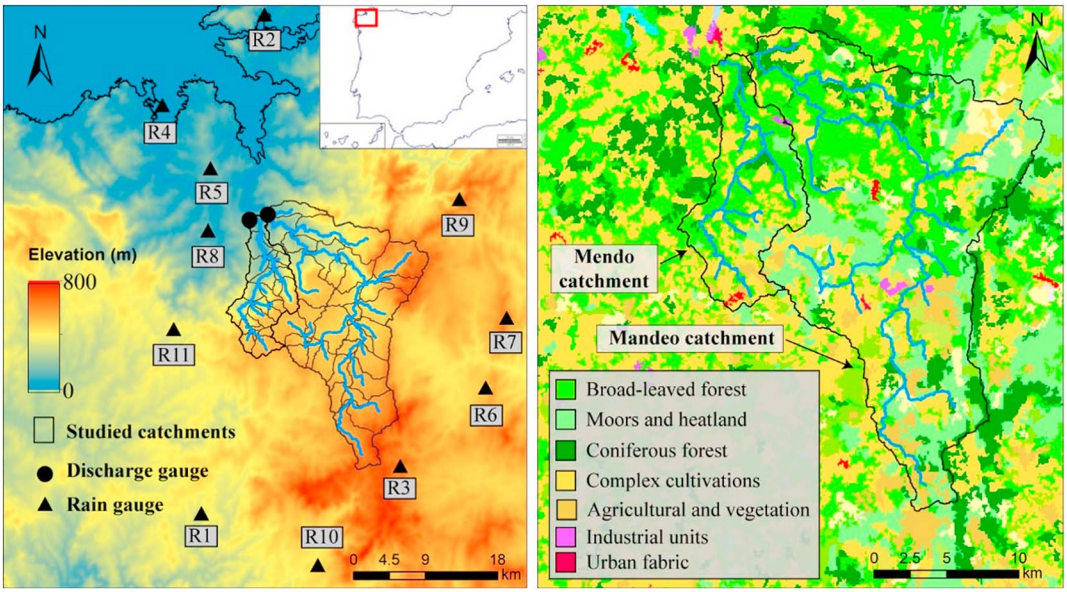

Figure 1. Study region and location of the 11 rain gauges. The Mandeo and Mendo catchments, as well as the subbasins included in the hydrological model, are shown in the left figure.

calibrated relation between the antecedent rainfall depth and the soil infiltration capacity during a storm event. The advantage of this technique over standard procedures is that it does not make strong assumptions about the spatial and temporal structure of rainfall and, at the same time, it naturally considers the combined effect of AMC and rainfall intensity.

The flood frequency estimates obtained with the proposed methodology are compared to those computed with a conventional method based on the evaluation of basin-averaged IDF curves and on the definition of synthetic design hyetographs. The analysis is presented in two watersheds located in northwestern Spain with drainage areas of 84 and 353 km^2, respectively. The results show that the conventional methodology is very sensitive to the AMC conditions assumed for a given return period, and it tends to overestimate the flood discharges when compared to the proposed approach. Since it is not straightforward to establish which AMC should be used when applying a conventional method, this results in a great source of uncertainty in the results.

The following of this paper is organized as follows. Section 2 describes the physical properties of the study catchments and the methodology proposed here to incorporate the combined effect of AMC and rainfall variability in flood frequency analysis. The results obtained in the two study catchments with the proposed and conventional methods are compared and discussed in section 3. Finally, the main conclusions and contributions of the paper are summarized in section 4.

2. Study Area and Methodology

2.1. Study Catchments and Available Data

The two catchments used as study cases are those of the rivers Mandeo and Mendo (Figure 1). Both of them are located in northwestern Spain and are affected by the energetic atmospheric interchanges between the tropical and the polar regions. This produces frequent adverse storm events characterized by a large spatial and temporal variability of rainfall (Cabalar-Fuentes, 2005). The areas of each catchment are 353 (Mandeo) and 84 km^2 (Mendo), while the lengths of the main rivers are roughly 50 (Mandeo) and 30 km (Mendo). Average annual rainfall is 1,260 (Mandeo) and 1,240 mm (Mendo).

Both are predominantly rural catchments in which forest and brushland are the most extended land uses. In the Mandeo catchment, the elevation varies from zero to 810 m above sea level, with an average elevation of 480 m and an average slope of 0.056. The elevation of the Mendo basin varies within 25 and 564 m, with an average elevation of 344 m and an average slope of 0.052.

Table 1
Pluviometers Used in the Present Study

Pluviometer		Measuring	Z	P_{annual}	P_{24}
Id	Name	since	(m)	(mm)	(mm)
R1	Arzúa	2009	362	1,484	84
R2	CIS Ferrol	2000	37	1,243	52
R3	Corno do Boi	2005	731	1,326	66
R4	Coruña Dique	2008	5	649	37
R5	Guísamo	2012	176	1,145	56
R6	Sambreixo	2000	496	1,040	55
R7	Vilalba	2001	684	1,186	56
R8	Mabegondo	2000	94	1,105	58
R9	Marco da Curra	2000	651	1,476	70
R10	Melide	2003	477	1,154	59
R11	Olas	2005	401	1,492	70

Note. Z = elevation, P_{annual} = average annual precipitation, P_{24} = average annual maximum rainfall depth in 24 hr.

The orography and the orientation of the hillslopes have relevant effects on the characteristics of the storm events in the study catchments. On one hand, both catchments have a NNW orientation, which is the most frequent direction of arrival of the low pressure fronts in this region of Spain. Therefore, the path of most of the arriving storms follows the upstream direction of the basins, which has an attenuation effect on the peak discharges (Liang & Melching, 2015). On the other hand, due to the steep orography of the hillslopes, the arriving low pressure fronts are quickly uplifted on their path through the catchment. This contributes to increase the spatial and temporal variability of rainfall during storm events (Cabalar-Fuentes, 2005). These effects have also been observed in other regions with similar climate and orography, such as the U.S. Pacific Coast (Eiras-Barca et al., 2016).

Historical rainfall data with a time resolution of 10 min is available from the rain gauge network of the regional meteorological agency MeteoGalicia. From this network, 11 tipping bucket pluviometers located around the catchments were selected in order to interpolate the rainfall fields (Figure 1 and Table 1). The average annual maximum rainfall depth in 24 hr (P_{24}) registered at each station varies between 37 and 84 mm. The average annual precipitation (P_{annual}) is strongly correlated with P_{24} ($r = 0.90$) and varies, with the exception of rain gauge R4, within 1,000 and 1,500 mm. Notice in Table 1 that the rain gauge density varies over the time period with available data. This implies that the most recent storms will have more realistic rainfall estimates than the earlier ones. Nonetheless, this does not pose a problem for the proposed methodology.

Radar data with spatial and temporal resolutions of 1 km and 5 min, respectively, are also available but only for a limited number of rainfall events. Due to its limited length, the radar data could not be used in the statistical analysis of rainfall. However, it was used to verify that the 11 available pluviometers are sufficient to represent the main features of the spatial structure of storm rainfall for aggregation levels larger or equal to 1 hr. This will be shown later on in section 2.2.2.

Daily peak discharges measured since 2010 at two gauge stations (one on each catchment) managed by the Regional Water Administration (Augas de Galicia) are also available. There is no detailed information about the accuracy and reliability of these data. A preliminary analysis revealed several incoherent records, characterized by very high peak discharges during low rainfall periods. Even if the most obvious erroneous data were filtered, the uncertainty on the remaining discharge data is probably large. Despite the limited accuracy ascribable to discharge measurements, the available data were used to do a rough calibration of the hydrological model, as it will be detailed in the following sections.

2.2. Proposed Methodology

The proposed methodology is based on the hydrological simulation of real storm events in the study catchments in order to obtain a series of flood peak discharges, which are then used to fit an extreme value distribution. The main steps of the methodology are listed below and described in the following of this section:

1. Select historical time series of rainfall data at an adequate time resolution for the study catchment.
2. Compute historical time series of precipitation averaged over the whole basin and over each of its main subbasins (those that will be included in the hydrological model).
3. Find and select potentially hazardous storm events from the basin-averaged time series of precipitation computed in step 2. This will typically be done using a peak-over-threshold criterion based on the rainfall depth. Since the river discharge depends not only on the total rainfall depth but also on the spatial and temporal variability of rainfall and on the AMC, it is convenient to define a relatively low peak-over-threshold (POT) and let the hydrological model determine the storm events that generate highest river discharges.
4. Model the selected storm events with a semidistributed or distributed hydrological model. The model must be able to account for the spatial variability of rainfall in the simulations (i.e., do not use the basin-averaged rainfall time series in the hydrological model but instead define spatially varying rainfall

fields from the available data). At this step, if some streamflow data are available, a relation between the antecedent rainfall depth and the infiltration parameters should be calibrated.

5. Extract the peak discharge for each rainfall event modeled in step 4, and fit an extreme value distribution to the discharge data. The flood discharge for different return periods can be evaluated from the fitted extreme value distribution.

2.2.1. Selection of Historical Time Series of Rainfall

The first step of the methodology is to obtain time series of rainfall that can be used to define its spatial and temporal variability at the event scale during a historical time period. Most commonly, these will be point rainfall data at several pluviometers located around and within the study catchment. In this case we have used the 11 pluviometers shown in Figure 1 and in Table 1. The historical data obtained in this features spatial and temporal variability in basin-scale rainfall, as represented by the observations from the rain gauges. In some cases there might be data from meteorological radars that can be combined with rain gauge data to obtain a more detailed characterization of the rainfall fields.

2.2.2. Basin-Averaged Time Series of Precipitation

The second step is to obtain basin-averaged and subbasin-averaged time series of precipitation from the available rainfall data. The data registered by the 11 pluviometers of MeteoGalicia were spatially interpolated using a natural neighbor interpolation and then averaged over the catchment surface. Other interpolation techniques, as nearest neighbor interpolation and ordinary kriging, were tested, with similar results. More accurate techniques such as kriging with external drift (KED) could not be used because the availability of radar data in the study region is limited and could not be applied systematically to interpolate the rainfall fields in the catchments. The spatial interpolation was done with a time resolution of 10 min, in order to obtain historical time series of basin-averaged precipitation at 10-min resolution. The basin-averaged time series of rainfall used in this work extended from 2001 to 2017 (17 years).

To verify the accuracy of the basin-averaged rainfall computed with natural neighbor interpolation, a number of storm events in which radar data were available were selected, and the KED interpolation was used to estimate the rainfall fields for those events. Time series of basin-averaged rainfall for the selected events computed with KED and natural neighbor interpolations are compared in Figure 2. There is a strong similarity between time series, especially for aggregation levels larger than 1 hr. For the 3-hr rainfall aggregation level, the correlation coefficient is equal to 0.99 and the mean absolute error of the order of 0.1 mm/hr. For a 0.5-hr rainfall duration, the discrepancies in the rainfall intensity is somewhat larger, but the dispersion around the 1:1 line is low (with correlation coefficients larger than 0.90 in all cases), and there is no significant bias (percent bias lower than 8%). Nonetheless, this timescale is not relevant given the size of the study catchments. In any case, as mentioned before, the radar data could not be included in our analysis since it is just available for a limited number of events. If available in other case studies, it can be easily included in the methodology in order to compute the basin-averaged rainfall time series.

2.2.3. Potentially Hazardous Rainfall Events

The historical basin-averaged 10-min series of rainfall were aggregated at different durations ranging from 1 to 24 hr (1, 3, 6, 12, 18, and 24 hr). From each of these, a number of potentially hazardous rainfall events were selected using the POT method. The threshold for each aggregation level was defined as 70% of the average annual maximum rainfall for that specific duration. A minimum 1-week lag was also imposed when applying the POT method. One week is not enough to assure statistical independence of two consecutive events. However, the storm events identified at this step will not be directly used to fit an extreme rainfall distribution but just as input data in a hydrological model. Therefore, the statistical independence of events is not relevant at this step. Conversely, it is difficult to assess a priori which rainfall events are more likely to generate high discharges, due to the intraevent variability of rainfall and to the role of the AMC. Thus, it is more convenient to remain nonrestrictive at this stage and to select all the events that can be considered potentially hazardous. Statistical independence of events will be imposed in later steps.

This criterion produced around 100 events in 17 years of available data (i.e., around six events per year). Other slightly different thresholds (between 50% and 90% of the average annual maximum rainfall) and minimum lags between events (from 5 to 15 days) were tested, with similar results at the end of the methodology.

2.2.4. Hydrological Modeling of the Potentially Hazardous Rainfall Events

From the previous step, a number of potentially hazardous storm events were obtained. These events were introduced in a hydrological model to obtain the corresponding flood hydrographs and peak discharges. We

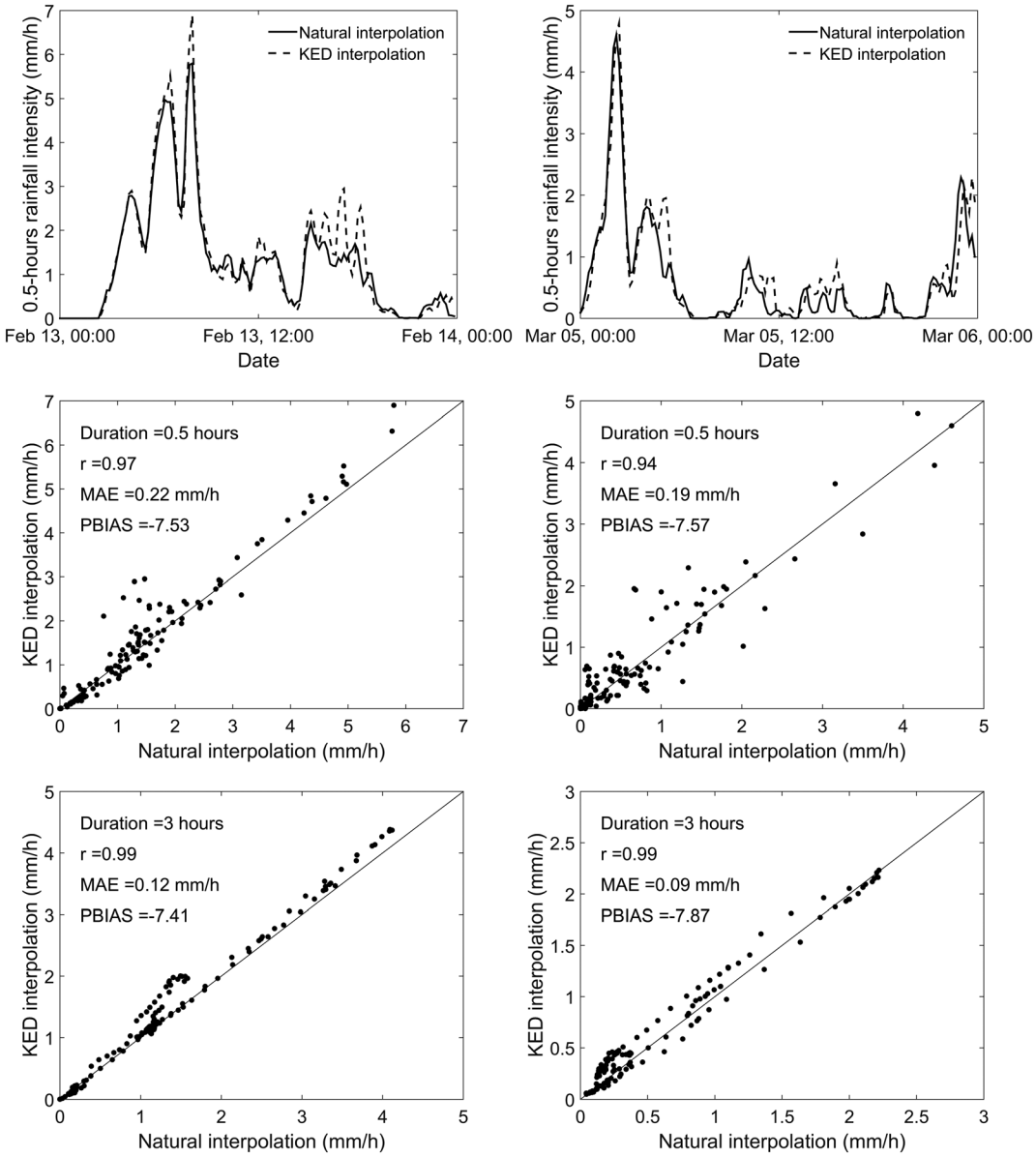

Figure 2. Comparison between basin-averaged rainfall obtained with natural neighbor interpolation from the pluviometers data and from kriging with external drift (KED) interpolation combining the pluviometers and radar data. *r* = Pearson correlation coefficient, MAE = mean absolute error, PBIAS = percent bias (Gupta et al., 1999).

have used the semidistributed model HEC-HMS v4.2.1 (Scharffenberg & Fleming, 2006), although any other semidistributed or distributed model could be used for the same purpose as long as the spatial variability of rainfall is considered in the model.

The geospatial hydrology toolkit HEC-GeoHMS (Fleming & Doan, 2009) was used to divide the study catchments in several subbasins, to generate the geometrical representation of the catchments in HEC-HMS, and to obtain the main features of each hydrological element (subbasin areas, reach lengths, and average slopes). The Mandeo catchment (353 km^2) was subdivided in 34 subbasins with areas ranging from 0.2 to 30 km^2, while the Mendo catchment (84 km^2) was discretized in 24 subbasins with areas ranging from 0.5 to 8 km^2.

The rainfall time series were defined individually for each subbasin, from the subbasin-averaged values obtained in step 2. In such a way, a realistic spatial and temporal structure of rainfall is included in the simulations.

Table 2
Catchment-Averaged Values of the Nine Curve Number (CN) Classes Considered in the Hydrological Model

CN class	CN1	CN2	CN3	CN4	CN5	CN6	CN7	CN8	CN9
Mandeo	51	56	61	66	71	76	80	85	90
Mendo	53	56	60	63	66	69	73	76	79

Rainfall-runoff transformation was computed with the SCS unit hydrograph. The lag time (T_{lag}) used in the SCS unit hydrograph was estimated as $T_{lag} = 0.6T_c$. The concentration time (T_c) of each subbasin was determined using the TR55 method (USDA, 1986). TR55 computes T_c as the sum of three travel times that correspond to sheet flow, shallow concentrated flow, and channel flow. Each of them is computed from the topographical features (slope, length, and area) and surface roughness (Manning coefficient) of the corresponding hydrological elements (hillslopes, shallow watercourses, and main channels). Using these estimations, the lag times computed for the different subbasins vary from 0.25 to 2.2 hr in the Mandeo catchment and from 0.3 to 1.5 hr in the Mendo catchment.

Flow routing along the main river network was computed using the kinematic wave equation. The average slope of the river reaches was obtained from the Digital Terrain Model (DTM). The average values of the cross-section width and Manning coefficient were determined from field inspection. Cross-section width varies from 5 to 10 m, while the Manning coefficient varies from 0.03 to 0.06.

Infiltration losses were evaluated using the curve number (CN) method. A reference CN was assigned to each subbasin according to its Hydrological Soil-Cover Complex (soil cover, practice, hydrological condition, and hydrological soil group) for average soil moisture conditions. Since the infiltration capacity of a soil is largely dependent on its AMC, the SCS defines three possible CN classes (dry, average, and moist) based on the cumulative 5-day antecedent rainfall depth before the storm event (R_5). Each CN class is defined by a factor that multiplies the reference CN corresponding to average AMC conditions. These factors depend on the CN itself and are lower than 1 (increase infiltration) for dry antecedent conditions and greater than 1 (reduce infiltration) for moist antecedent conditions.

The CN classes proposed by the SCS can be used if no calibration data at all is available at the study site. In our case, there are two gauging stations, one on each catchment, with daily peak discharge data since 2010. These data were used to calibrate a relation between different CN classes and the antecedent rainfall depth. This was the only calibration performed on the hydrological model. The procedure followed is slightly different to the standard SCS procedure and is therefore detailed in the following.

The reference CN, as well as the moist and dry AMC factors recommended by the SCS, was estimated individually for each subbasin defined in the hydrological model. This gives three CN classes corresponding to dry, average, and moist conditions, each one representing a spatial distribution of CN in the catchment. For each subbasin, six additional CN classes were defined (three CN classes between the dry correction and the reference value, and three values between the reference value and the moist correction). The CN values for each of these classes were linearly interpolated from the SCS recommended values. This gives nine possible CN values for each subbasin. The catchment-averaged values of CN corresponding to the nine classes are shown in Table 2. Notice that only the catchment-averaged values are shown in the table for the sake of conciseness, but each subbasin has its own value of CN according to the Hydrological Soil-Cover distribution. In Table 2, the classes CN1, CN5, and CN9 correspond respectively to the SCS values for dry, normal, and moist AMC.

Once the nine CN classes are defined, they must be related to the AMC of the soil. In order to do so, a number of calibration events were selected from the available observed data. The calibration events were chosen as those with available measured discharge data and at the same time classified as potentially hazardous according to the criterion defined in step 3. This produced around 30 calibration events for each catchment. The HMS model was run nine times for each calibration event (one run for each possible CN class). The peak discharges obtained with the model were compared to the measured ones in order to establish, for each rainfall event, the CN class that gives the best agreement with the observed data. The optimum CN classes obtained in this way were plotted against the antecedent rainfall depth in the n previous days (with varying values of n between 1 and 120 days), and the following power regression was fitted to the data:

$$CN_{class} = \text{round}\left(a \cdot R_n^b\right) \quad (1)$$

where R_n is the rainfall depth on the n previous days, a and b are the constant parameters of the power regression, and CN_{class} is an integer value between 1 and 9. From the n possible power regressions, the one with the best agreement between numerical and observed peak discharges in terms of the

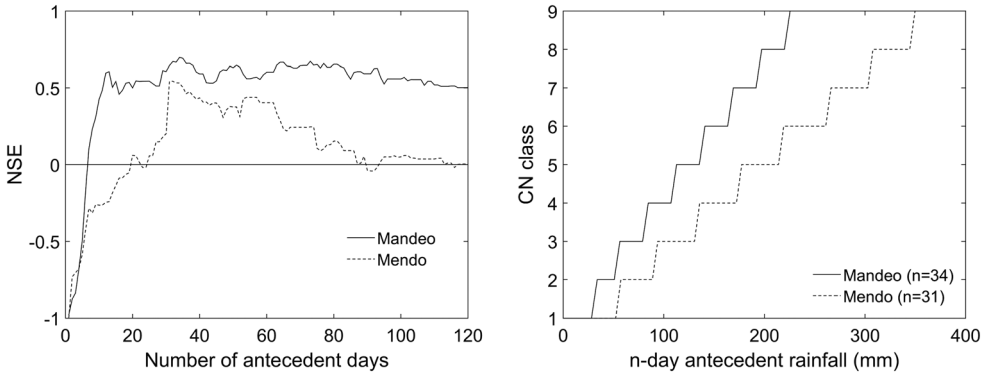

Figure 3. Agreement between numerical and observed peak discharges in terms of Nash-Sutcliffe efficiency (NSE) as a function of the number of antecedent days considered in equation (1) (left), and relation between CN_{class} and *n* day antecedent rainfall depth that gives the best agreement (right).

Nash-Sutcliffe Efficiency (Nash & Sutcliffe, 1970) was chosen in order to relate the CN classes with its *n*-day antecedent rainfall. This procedure was done independently for the Mandeo and Mendo catchments (Figure 3).

Following this methodology, in the Mandeo catchment, the best predictor of CN_{class} was found to be R_{34} (i.e., the 34-day antecedent rainfall depth). In the Mendo catchment, the best calibration was obtained with R_{31}. In both cases, using R_5 produced a significantly worse calibration. The fitted regressions for each catchment are shown in Figure 3 and are given by

$$CN_{class,Mandeo} = \text{round}\left(0.078 \cdot R_{34}^{0.868}\right) \quad (2)$$

$$CN_{class,Mendo} = \text{round}\left(0.037 \cdot R_{31}^{0.928}\right) \quad (3)$$

The relations given by equations (2) and (3) are the only ones obtained from model calibration. Using R_{34} and R_{34} as the CN_{class} predictors is coherent with the results obtained by Schulze (1982), who found that in humid regions (as it is the study region), using the 30-day antecedent rainfall as a predictor of the AMC when applying the SCS method produced better results than using a 5-day period. Similar findings were reported by Hope and Schulze (1982), who used a 15-day antecedent period when applying the SCS method to humid regions of South Africa.

The CNs derived via calibration using the previous methodolgy differ substantially from the CNs that would be assigned from standard guidance, as shown in Figure 4. The correlation between both values of CN is not significant, and the differences are quite relevant. This means that the methodology proposed here needs some streamflow data in order to calibrate a relation between CN and some predictor of the soil moisture

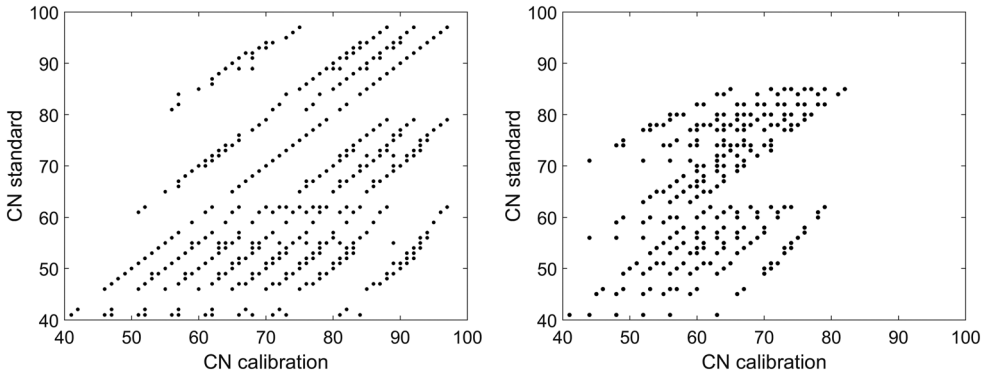

Figure 4. Scatterplot comparing the curve numbers (CNs) derived via calibration with the CNs that would be used from standard guidance in the Mandeo (left) and Mendo (right) catchments. Each scatterpoint represents the CN assigned to a specific subbasin of the hydrological model during a specific calibration event.

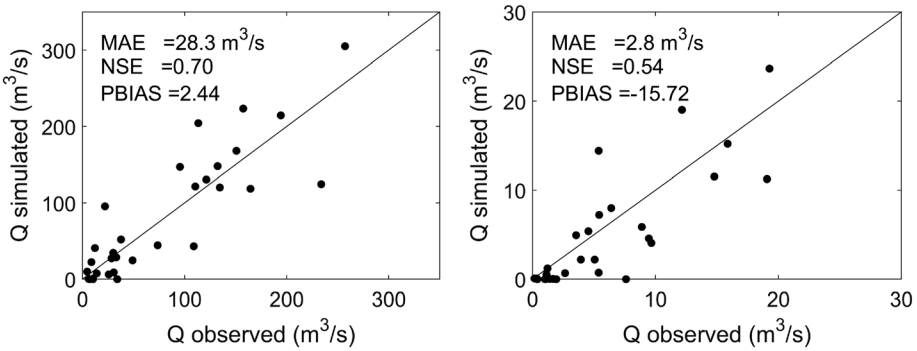

Figure 5. Agreement between the observed and simulated peak discharges in the Mandeo (left) and Mendo (right) catchments. MAE = mean absolute error, NSE = Nash-Sutcliffe efficiency, PBIAS = percent bias (Gupta et al., 1999).

conditions. Otherwise, rainfall-runoff transformation will not be properly represented by the hydrological model.

The measured peak discharges versus the ones predicted with HEC-HMS for the calibration events using equations (2) and (3) are shown in Figure 5, together with the following performance measures:

$$\mathrm{NSE} = 1 - \frac{\Sigma_{i=1}^{n}\left(Q_{p,i}^{\mathrm{HMS}} - Q_{p,i}^{\mathrm{exp}}\right)^2}{\Sigma_{i=1}^{n}\left(Q_{p,i}^{\mathrm{exp}} - \overline{Q_{p}^{\mathrm{exp}}}\right)^2} \qquad \mathrm{MAE} = \frac{\Sigma_{i=1}^{n}\left|Q_{p,i}^{\mathrm{HMS}} - Q_{p,i}^{\mathrm{exp}}\right|}{n} \qquad \mathrm{PBIAS} = 100\,\frac{\Sigma_{i=1}^{n}\left(Q_{p,i}^{\mathrm{HMS}} - Q_{p,i}^{\mathrm{exp}}\right)}{\Sigma_{i=1}^{n} Q_{p,i}^{\mathrm{exp}}} \quad (4)$$

where n is the number of calibration events, $Q_{p,i}^{\mathrm{HMS}}$ is the peak discharge computed with HEC-HMS for each calibration event, and $Q_{p,i}^{\mathrm{exp}}$ is the measured peak discharge for each calibration event.

Once the relations between the antecedent rainfall and CN are established from the calibration events, equations (2) and (3) are used to assign a CN class to each one of the potentially hazardous rainfall events identified in step 3. These are modeled in HEC-HMS, using the measured temporal and spatial variability of rainfall in the catchments, to obtain the estimated peak discharge for each potentially hazardous rainfall event.

It should be noticed that the antecedent rainfall is chosen as the predictor of the CN because the infiltration capacity of the soil depends largely on the initial soil moisture conditions, which in general are strongly related to the rainfall depth during the days previous to the flood event. However, the present availability of satellite data opens up the possibility of using directly the soil moisture content, instead of the antecedent rainfall, as the predictor of the CN for each storm event. To explore this possibility, we have used the satellite data from the Soil Moisture Active Passive (SMAP) mission, which gives estimations of the soil moisture content at a 10-km resolution. Figure 6 shows the CN calibrated with the proposed methodology

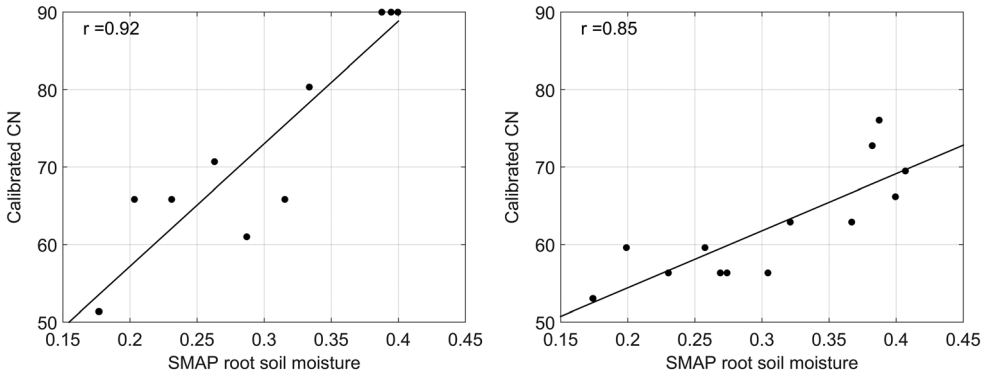

Figure 6. Soil Moisture Active Passive (SMAP) root soil moisture versus calibrated curve number (CN) in the storm events identified since 2015 (available SMAP data). Mandeo (left) and Mendo (right) catchments.

in the storm events registered since 2015, against the root soil moisture obtained from SMAP at the beginning of those events. The correlation coefficient between both variables is very high (0.92 in the Mandeo and 0.85 in the Mendo), which suggests that soil moisture data obtained from SMAP has a great potential to be used as an efficient predictor of the CN in future applications of the methodology. However, SMAP data are only available since 2015, and therefore, it could not be fully incorporated in the study cases presented in this paper. Therefore, in the present study, we have maintained the antecedent rainfall to derive the CN.

2.2.5. Extreme Value Distribution of the Peak Discharge

The peak discharges obtained with HEC-HMS for each event identified in step 3 were used to estimate the annual exceedance probability distribution of discharge at both catchments. To do so, the POT method was applied to the modeled peak discharges in order to obtain a statistically independent sample of flood discharges. This is necessary because (1) not all the potentially hazardous rainfall events produce high discharges and (2) the lag period used for the selection of rainfall events in step 2 is too small to ensure statistical independence. The POT method was applied with a threshold equal to 50% of the average annual maximum discharge and a minimum lag period between flood events of 1 month. This criterion produced roughly one flood event per year.

Once the peak discharges sample was obtained, the exceedance probability of each discharge was estimated using the plotting position formula of Gringorten (1963), and an extreme value distribution was fitted to the data. The formula of Gringorten is optimized to plot the largest observations of a Gumbel distribution. However, it is common in practice to try several extreme value distributions and select the one that gives the best fit to the data. In this case we have tested the two-parameter Gumbel distribution and the three-parameter Generalized Extreme Value distribution. A three-parameter distribution is more flexible to fit the data, but it is also more sensitive to outlying events, since it can easily follow singularities of the data set (Cunnane, 1985). Some water administrations recommend using a three-parameter distribution only when the length of the measured data exceeds a minimum number of 50 years (Midttømme et al., 2011). Otherwise, a two-parameter distribution is preferred. Taking into account the previous considerations, the Gumbel distribution was chosen to characterize the extreme flood discharge at both catchments.

2.3. Conventional Methodology

Conventional methods used in flood frequency analysis from rainfall data are based on the evaluation of IDF curves and on the definition of synthetic hyetographs for the study region. The practical application of conventional methods might differ in details such as the way in which the IDF curves are computed, the shape and parameters used to define the synthetic hyetographs, the definition of ARF, or the way in which rainfall is distributed over the study catchment. The main drawbacks of conventional methods have been discussed in the section 1 and originate mainly from the fact that they do not account properly for the real temporal and spatial structure of rainfall during storm events, nor for the AMC of the soil. These drawbacks have already been pointed out by other researchers (Wright et al., 2014a).

In this study we have used a conventional method based on the estimation of basin-averaged IDF curves for the study catchments and on the definition of synthetic hyetographs for a given return period using the ABM. Those are quite standard procedures in flood frequency analysis. The specific implementation used in this study is described in the following of this section. The same raw rainfall data were used in the proposed and conventional methods.

2.3.1. Basin-Averaged IDF Curves

The IDF curves were computed from the historical time series of basin-averaged rainfall at 10-min resolution, computed as detailed in section 2.2.2. This was done independently for the Mandeo and Mendo catchments. In addition, and just for comparison purposes, we have computed the IDF curves at each of the 11 rain gauge stations (i.e., using just the rainfall data registered by each station). Using basin-averaged and site-specific IDF curves takes into account the spatial variability of rainfall in the study catchment and avoids the need of using generic ARF derived for other catchments or regions. Notice that very often in practice, conventional methods are applied using generic ARF, at best derived for the climatic region where the study catchment is located. Those kinds of implementations based on ARF account for point-to-area rainfall differences, but they do not include the spatial variability of rainfall in the hydrological simulations.

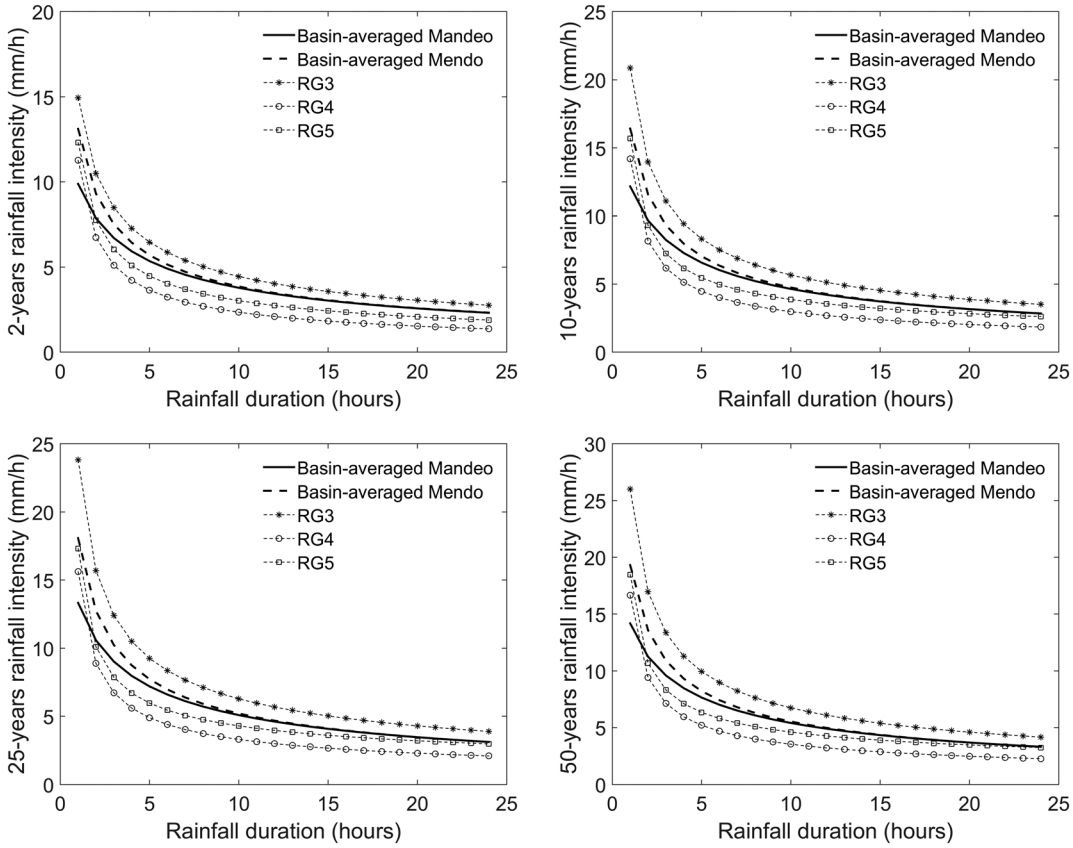

Figure 7. Estimated catchment-averaged intensity-duration-frequency curves corresponding to return periods of 2, 10, 25, and 50 years.

The POT method was applied to the basin-averaged time series considering different rainfall aggregation levels (durations of 0.5, 1, 3, 6, 12, 18, and 24 hr). For each aggregation level, the rainfall threshold was defined as 70% of the average annual maximum rainfall depth for that specific duration. The minimum lag period between peaks was established as 30 days. This criterion produced around 70 rainfall events on each catchment. For each duration, the exceedance probability of the sampled data was estimated using the formula of Gringorten (1963). Following the considerations mentioned in section 2.2.5, three candidate extreme value distributions were tested: Gumbel (two parameters), sqrtETmax (two parameters), and Generalized Extreme Value (three parameters). The sqrtETmax (SQRT-Exponential Type Distribution of Maximum) was proposed in Etoh et al. (1987) specifically for annual maximum series of total rainfall depth during a single rainstorm or rainfalls of about 24 hr.

The best fit to the data was obtained with the Gumbel distribution, and it was therefore the one used to compute the IDF curves shown in Figure 7. Due to the relatively short length of the available time series (17 years), the IDF curves were only computed for return periods of up to 50 years. It is remarkable in Figure 7 the differences between the basin-averaged IDFs and those estimated from point rainfall measurements at each station. This is in direct relation with the ARF. For short rainfall durations, the point rainfall intensities are in general larger than the basin-averaged intensities because the maximum rainfall does not occur over the whole catchment simultaneously. The differences in the point rainfall IDFs is due to the nonhomogeneity of the statistical characteristics of rainfall over the study region (see Table 1). For those small aggregation levels, the basin-averaged intensities in the Mendo catchment are larger than in the Mandeo catchment because the later one has a larger surface, and thus, the ARF is smaller. For larger aggregation levels, the basin-averaged IDF in the Mandeo and Mendo tend to the same value because the spatial correlation of rainfall increases with the rainfall duration. Those differences are reflected in the basin-averaged design hyetograph computed with the ABM (Figure 8), which has a higher peak intensity in the smaller catchment (Mendo).

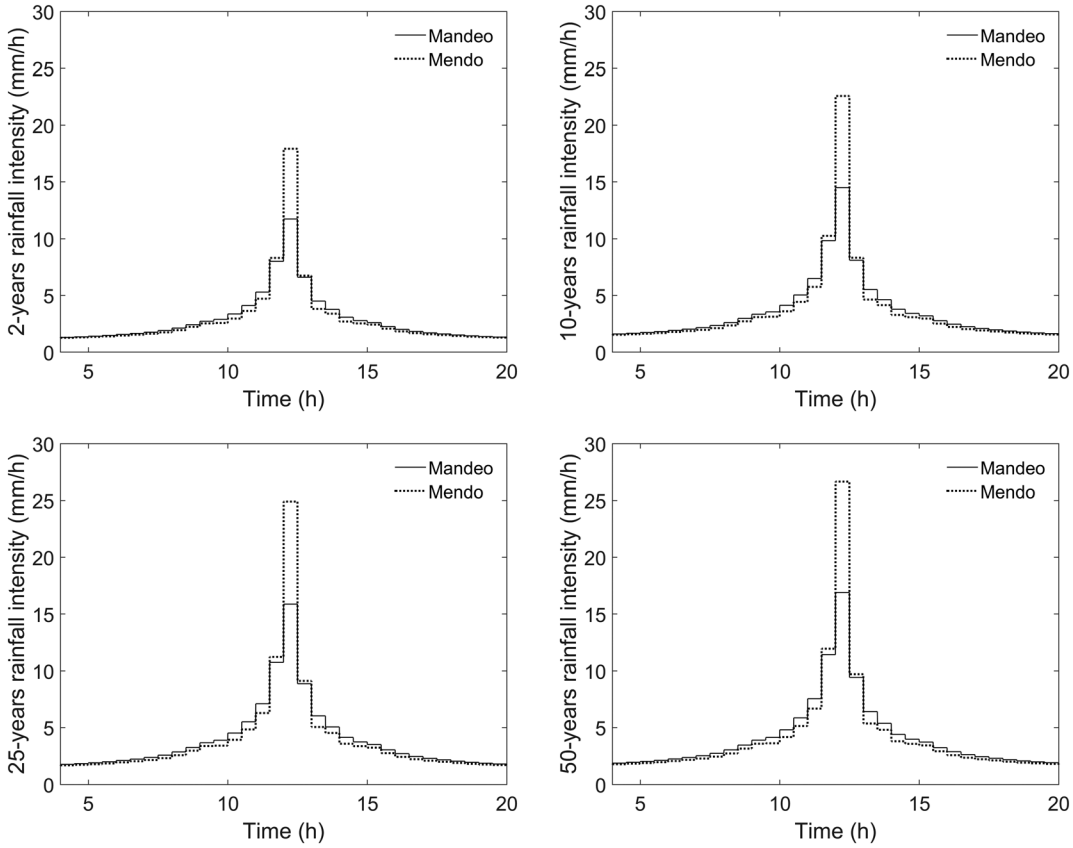

Figure 8. Catchment-averaged synthetic hyetographs for return periods of 2, 10, 25, and 50 years.

2.3.2. Synthetic Hyetographs

From the basin-averaged IDFs, the synthetic hyetographs for return periods of 2, 10, 25, and 50 years were defined using the ABM (Figure 8). The block duration was fixed to 0.5 hr in all cases, which is short enough given the estimated concentration time of the catchments (10 and 5 hr).

The hyetographs shown in Figure 8 were used as the rainfall input in HEC-HMS, in order to compute the flood discharge for different return periods using the conventional approach. The discretization and parameters introduced in HEC-HMS models are the same as those used in the proposed methodology, in order to restrict the differences between approaches to the way in which rainfall variability and AMC is considered.

3. Results and Discussion

3.1. Estimation of Flood Frequency

The flood discharges obtained with the proposed and conventional methods described in the previous section were compared for several return periods. The aim of this comparison is to analyze and quantify the relevance of considering site-specific rainfall patterns during storm events. Hence, the same hydrological model (same structure and same parameters) was used in both approaches. The model structure and parameters were already described in section 2.2.4. The only difference in the parameterization used with both methodologies is the definition of the CN, since the proposed approach accounts for the variability of AMC, while the conventional method does not. Therefore, we have applied the conventional approach using the three AMC considered in the SCS method (dry, normal, and moist), in order to compare the results with those of the proposed methodology. For comparison purposes, we have also computed the flood discharges using the RFFA at the global scale presented in Smith et al. (2015), which only requires the location, area, and average annual precipitation in the study basins.

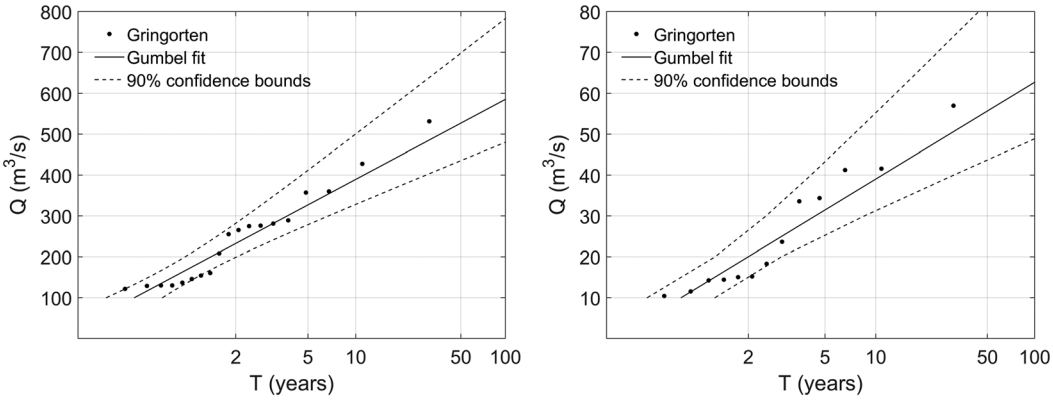

Figure 9. Exceedance probability of flood discharge data and fitted Gumbel distribution in the Mandeo (left) and Mendo (right) catchments, computed with the proposed methodology.

Figure 9 shows the Gumbel distribution fitted to the daily peak discharge, computed for the Mandeo and Mendo catchments following the proposed methodology. The flood discharges given by the Gumbel distribution for the return periods of 2, 10, 25, and 50 years are shown in Table 3 and vary between 232 and 527 m^3/s in the Mandeo catchment and from 20 to 56 m^3/s in the Mendo catchment. Notice that the 90% confidence intervals in Figure 9 are rather large, especially for the highest return periods, due to the low number of sample data (the whole study is done with 17 years of available rainfall data). If more years of rainfall data were available, the confidence intervals should reduce.

The standard approach is strongly dependent on the chosen AMC (dry, normal, or moist). In general, in the study region the maximum river discharges occur in the wet season, when the soil is under normal or moist conditions. As it could be expected, the dry AMC underestimates the flood discharges in all cases, and therefore, it should not be used in a flood frequency analysis. However, it is difficult to determine a priori which of the other two AMC conditions (normal or moist) is preferable to use in a conventional flood frequency analysis. In the Mandeo catchment, for instance, the normal AMC underestimates the flood discharges roughly by a factor 2 when compared to the proposed methodology. Conversely, the moist AMC overestimates the discharge, especially for low return periods. On the Mendo catchment, the normal AMC gives very similar results to the proposed method, while the moist conditions strongly overestimate the flood discharge (always when compared to the proposed method).

In addition, the chosen AMC has a large impact on the results, making the flood discharge estimation very sensitive to the decision of using one or another AMC. Discharges computed assuming moist conditions are, on average, three times larger than those computed assuming normal conditions.

Figure 10 shows the relation between the observed peak discharges and the antecedent rainfall depth for different number of antecedent days (5 and 34 days in the Mandeo and 5 and 31 days in the Mendo). The 5-day antecedent rainfall (R_5) is the one used in the standard application of the SCS method, while the 34-

Table 3
Daily Peak Discharges for Different Return Periods, Estimated With the Proposed and Standard Methodologies, as Well as With the Regional Flood Frequency Analysis (RFFA) at the Global Scale of Smith et al. (2015)

T	Mandeo—Q_T (m^3/s)					Mendo—Q_T (m^3/s)				
(years)	Proposed	Standard dry	Standard normal	Standard moist	RFFA	Proposed	Standard dry	Standard normal	Standard moist	RFFA
2	232	0	92	411	167	20	2	16	76	25
10	389	17	169	558	326	39	6	38	126	49
25	468	26	214	634	414	49	9	52	155	62
50	527	34	250	690	482	56	12	65	176	72

Note. Results obtained with the standard methodology are shown for the three different soil moisture content conditions considered in the Soil Conservation Service curve number method (dry, normal, and moist).

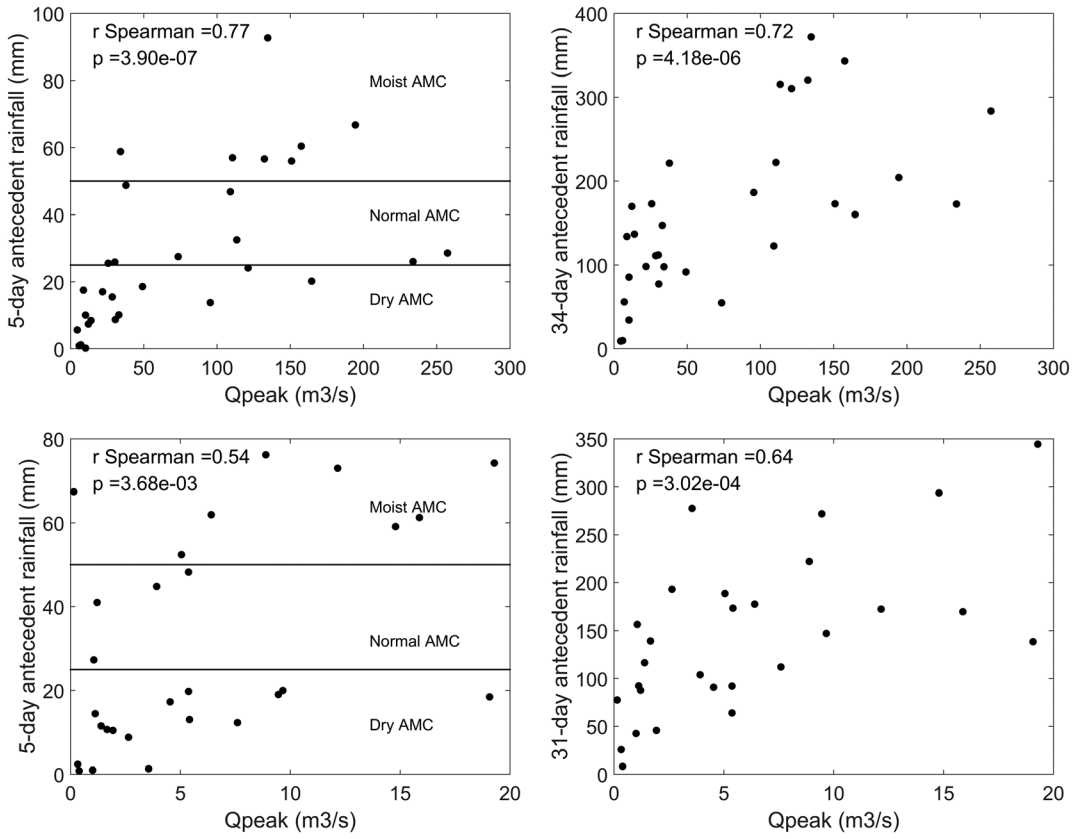

Figure 10. Observed peak discharge measured at the gauge stations of Mandeo (upper) and Mendo (lower) catchments versus antecedent rainfall. The correlation coefficient between antecedent rainfall and peak discharge is indicated (*r*).

and 31-day antecedent rainfall (R_{34} and R_{31}) are the ones used in equations (2) and (3) of the proposed methodology to estimate the infiltration parameter CN for each rainfall event. Figure 10 shows that in both catchments, there is a significant correlation between Q_p and the antecedent rainfall depth (R_{34}, R_{31}, or R_5). The Spearman's rank-order correlation coefficients vary between 0.54 and 0.77, with significance levels (*p* value) lower than 0.005 in all cases. This is coherent with the results shown in Figure 3 and reinforces the importance of considering the correct AMC. Despite this correlation, Figure 10 also emphasizes that the highest peak discharges do not always occur under the same AMC conditions, and thus, it is important to consider event-specific AMC, or at least the possible combinations of AMC and rainfall intensity.

Coming back to the conventional approach applied to the study basins, if we estimate the AMC according to R_5 and Figure 10, in the Mendo catchment we would say that the moist AMC is the most appropriate to estimate flood discharges. However, as shown in Table 3, this would produce discharges that are three times larger than those obtained with the proposed methodology. Moreover, given the increasing trend between the antecedent rainfall and the peak discharge shown in Figure 10, the AMC that should be considered in a conventional method should be dependent on the return period. Compared to the standard approaches, the proposed methodology has the advantage that it incorporates in a natural way the AMC in order to establish the infiltration parameters to be used during each potentially hazardous storm event.

Table 3 also presents the flood discharges computed with the RFFA at the global scale presented in Smith et al. (2015). The results of Smith et al. (2015) were obtained using a global database of discharge data and depend only on the catchment area, average annual rainfall, and climate region. This method can therefore be applied to any region in the world provided that the drainage area and average annual precipitation in the basin are known. In our case, both study basins are in the temperate climate zone. The flood discharges obtained (Table 3) lie within the ones computed with the conventional methodology using normal and moist AMC conditions. This is physically coherent since, as mentioned before, in humid regions it is expected that

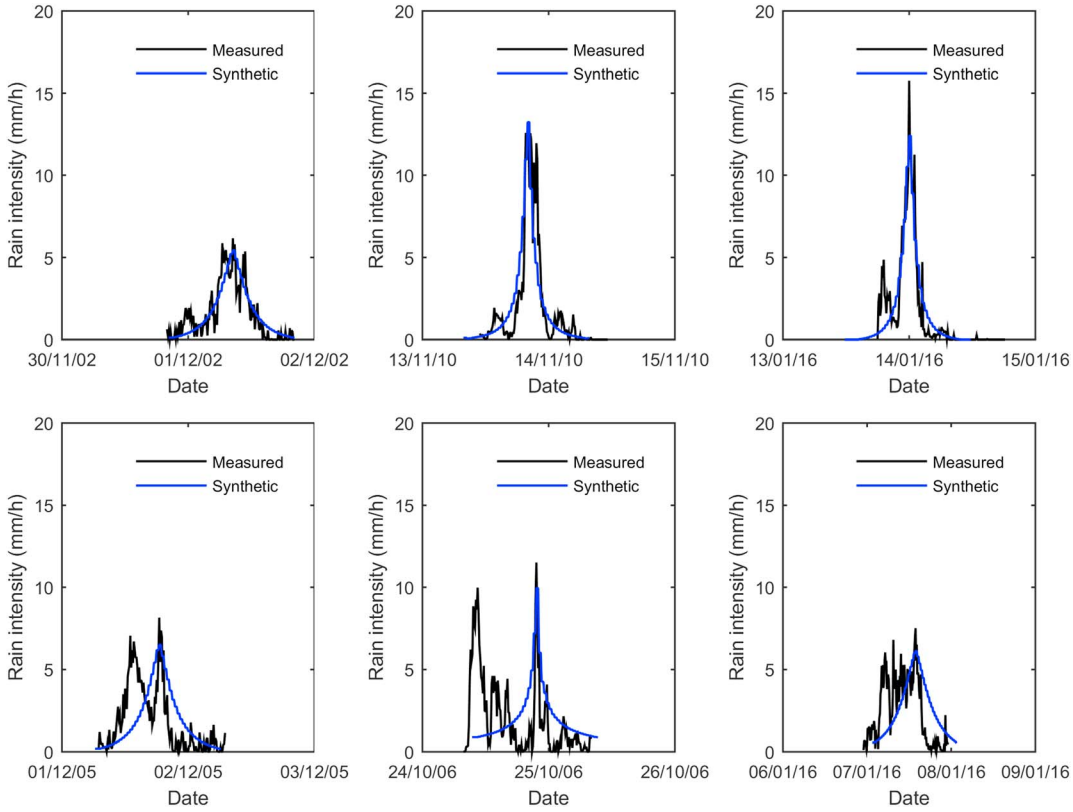

Figure 11. Comparison of real and synthetic alternating block hyetographs for several events.

flood discharges occur when the AMC are somewhere between normal and moist. Moreover, RFFA discharges are quite similar to the ones obtained with the proposed methodology, with absolute relative differences within 10% and 30%, which is remarkable considering that the regional regressions presented in Smith et al. (2015) have been developed at a global scale.

3.2. Relevance of the Intraevent Temporal Variability of Rainfall

In order to further analyze the relevance of the temporal variability of rainfall in the evaluation of peak discharges, an equivalent synthetic hyetograph was computed for each of the potentially hazardous events. This was done by first computing the intensity-duration curve of each event and then applying the ABM with that intensity-duration curve. The alternating block hyetograph computed for each event in such a way has the same maximum intensities that the real event for duration periods of 0.5, 1, 2 h, etc. The only difference between the real and the alternating block hyetographs is the way in which rainfall intensities are organized in time. Figure 11 shows the real and synthetic alternating block hyetographs computed for several representative events. In some events, both hyetographs are quite similar. This is for instance the case of the events occurring on 01 December 2012, 14 November 2010, and 14 January 2016 in Figure 11. However, in other events the difference between real and synthetic hyetographs is remarkable. Some events have two peak intensities that cannot be captured by the alternating block hyetograph (e.g., those of 02 December 2015 and 25 October 2006), while in other events, the intensity remains with almost constant high values during several hours (e.g., on the event of 07 January 2016). In order to quantify the effect that these differences in the temporal pattern of rainfall have on the computed peak discharges, the synthetic hyetographs for all the potentially hazardous events were modeled with HEC-HMS, using exactly the same hydrological parameters (including the same CN) as in the real events. As shown in Figure 12, it is not evident whether the alternating block hyetograph is more or less conservative than the real measured hyetographs. Actually, in some events the alternating block hyetograph produces higher peak discharges, while in others it predicts lower discharges, without a clear trend between these differences and the peak discharge. It is remarkable that the peak discharge estimates obtained with the ABM are unbiased with respect to the ones obtained with the

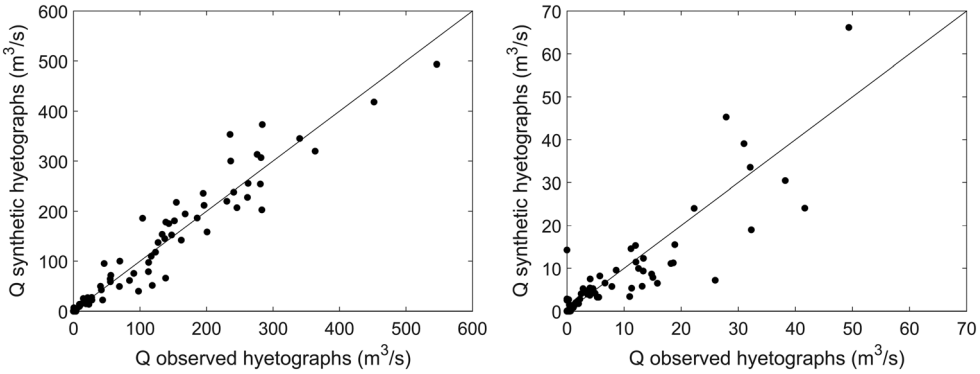

Figure 12. Comparison of peak discharges for each rainfall event computed using the measured hyetographs and the alternating block hyetographs.

observed hydrographs, and the dispersion on the data shown in Figure 12 is relatively low. This suggests that intraevent temporal variability might not be so relevant in this case.

4. Conclusions

The two most important processes when modeling rainfall-runoff transformation during storm events are rainfall and infiltration. However, the methods commonly used to estimate the frequency of flood discharges in poorly gauged basins make strong simplifications regarding these two processes. Compared to conventional methods, the methodology proposed in this paper accounts for the observed intraevent spatial and temporal variability of rainfall, as well as for site-specific antecedent soil moisture conditions. For these reasons, it provides a more site-specific representation of rainfall-runoff transformation than conventional methods.

Conventional design storm methods assume that a basin-average *T*-year rainfall falls uniformly over the whole catchment. Even if ARF or similar techniques can be used to transform point rainfall to basin-averaged precipitation, the hypothesis of a spatially uniform rainfall remains unrealistic. The proposed methodology copes with this problem by working with the observed spatial and temporal variability of rainfall as represented by the available rain gauge data.

Another problem when using conventional methods is to determine the soil infiltration parameters that should be considered in the hydrological model, since infiltration is strongly dependent on the AMC, which might vary from one storm to another. In the study basins, the maximum peak discharges do not always occur when the soil is under moist conditions, and this makes it difficult to decide which AMC should be considered when applying the conventional methodology. However, this decision has a very high impact on the computed flood discharges. In the study basins, there is a factor 3 between the discharges computed assuming either normal or moist AMC. By modeling each storm event independently, the proposed method accounts in a natural way for the AMC without making additional hypothesis. In the simulations presented here, antecedent rainfall is used to account for AMC. However, the recent availability of satellite soil moisture data from the SMAP mission opens up the possibility of using these data instead of antecedent rainfall to account directly for AMC in future studies.

The main shortcoming of the proposed methodology is that it requires some streamflow data in order to calibrate the relation between antecedent rainfall and CN. This prevents its applicability to basins with no discharge data at all. In order to extend the applicability of the method from poorly gauged basins to ungauged basins, a geographically generalizable relationship between antecedent rainfall and CN would be required. This possibility should be explored in the future through the application of the method to a much larger number of catchments.

Given the last developments in hydrological models and the increasing capacity of computers, we consider that flood frequency analysis in poorly gauged basins should focus on incorporating an accurate

representation of rainfall and infiltration during individual storm events, rather than in the definition of specific design storms or AMC for a given return period.

Acknowledgments
This work was financially supported by the Spanish Ministry of Economy and Competitiveness (Ministerio de Economía y Competitividad) within the project "CAPRI: Probabilistic flood prediction with high resolution hydrologic models from radar rainfall estimates" (CGL2013-46245-R). Ignacio Fraga received financial support from the Xunta de Galicia (Centro Singular de Investigación de Galicia accreditation 2016–2019) and the European Union (European Regional Development Fund-ERDF). The historical rainfall data from the pluviometers used in this work, as well as the discharge data at the two gauge stations, can be freely downloaded from the webpage of the Galician Meteorological Agency MeteoGalicia (http://www.meteogalicia.gal/observacion). The DTM of both catchments can be freely downloaded from the webpage of the Centro Nacional de Información Geográfica (http://centrodedescargas.cnig.es).

References

Allen, R. J., & DeGaetano, A. T. (2005). Areal reduction factors for two eastern United States regions with high rain-gauge density. *Journal of Hydrologic Engineering*, *10*(4), 327–335.

Asquith, W. H., & Famiglietti, J. S. (2000). Precipitation areal-reduction factor estimation using an annual-maxima centered approach. *Journal of Hydrology*, *230*(1–2), 55–69. https://doi.org/10.1016/S0022-1694(00)00170-0

Bacchi, B., & Ranzi, R. (1996). On the derivation of the areal reduction factor of storms. *Atmospheric Research*, *42*(1–4), 123–135. https://doi.org/10.1016/0169-8095(95)00058-5

Blazkova, S., & Beven, K. (2004). Flood frequency estimation by continuous simulation of subcatchment rainfalls and discharges with the aim of improving dam safety assessment in a large basin in the Czech Republic. *Journal of Hydrology*, *292*(1–4), 153–172. https://doi.org/10.1016/j.jhydrol.2003.12.025

Brocca, L., Melone, F., & Moramarco, T. (2011). Distributed rainfall-runoff modelling for flood frequency estimation and flood forecasting. *Hydrological Processes*, *25*(18), 2801–2813. https://doi.org/10.1002/hyp.8042

Cabalar-Fuentes, M. (2005). Los temporales de lluvia y viento en Galicia. Propuesta de clasificación y análisis de tendencias (1961-2001). *Investigaciones Geográficas (Esp)*, 36.

Camici, S., Tarpanelli, A., Brocca, L., Melone, F., & Moramarco, T. (2011). Design soil moisture estimation by comparing continuous and storm-based rainfall-runoff modeling. *Water Resources Research*, *47*, W05527. https://doi.org/10.1029/2010WR009298

Cunnane, C. (1985). Factors affecting the choice of distribution for flood series. *Hydrological Sciences Journal*, *30*(1), 25–36. https://doi.org/10.1080/02626668509490969

Dawdy, D. R., Griffis, V. W., & Gupta, V. K. (2012). Regional flood-frequency analysis: How we got here and where we are going. *Journal of Hydrologic Engineering*, *17*(9), 953–959. https://doi.org/10.1061/(ASCE)HE.1943-5584.0000584

De Lima, J. L. M. P., & Singh, V. P. (2002). The influence of the pattern of moving rainstorms on overland flow. *Advances in Water Resources*, *25*(7), 817–828. https://doi.org/10.1016/S0309-1708(02)00067-2

Eiras-Barca, J., Brands, S., & Miguez-Macho, G. (2016). Seasonal variations in North Atlantic atmospheric river activity and associations with anomalous precipitation over the Iberian Atlantic Margin. *Journal of Geophysical Research: Atmospheres*, *121*, 931–948. https://doi.org/10.1002/2015JD023379

Etoh, T., Murota, A., & Nakanishi, M. (1987). SQRT-exponential type distribution of maximum. In V. P. Singh (Ed.), *Hydrologic frequency modeling* (pp. 253–264). Dordrecht: Springer. https://doi.org/10.1007/978-94-009-3953-0_17

Falter, D., Schröter, K., Dung, N. V., Vorogushyn, S., Kreibich, H., Hundecha, Y., et al. (2015). Spatially coherent flood risk assessment based on long-term continuous simulation with a coupled model chain. *Journal of Hydrology*, *524*, 182–193. https://doi.org/10.1016/j.jhydrol.2015.02.021

Fleming, M. J., & Doan, J. H. (2009). *HEC-GeoHMS geospatial hydrologic modelling extension: User's manual version 4.2*. Davis, CA: US Army Corps of Engineers, Institute for Water Resources, Hydrologic Engineering Centre.

Gringorten, I. I. (1963). A plotting rule for extreme probability paper. *Journal of Geophysical Research*, *68*(3), 813–814. https://doi.org/10.1029/JZ068i003p00813

Gupta, H. V., Sorooshian, S., & Yapo, P. O. (1999). Status of automatic calibration for hydrologic models: Comparison with multilevel expert calibration. *Journal of Hydrologic Engineering*, *4*(2), 135–143. https://doi.org/10.1061/(ASCE)1084-0699(1999)4:2(135)

Hansen, E. M., L. C. Schreiner, and J. F. Miller (1982), *Application of probable maximum precipitation estimates: United States east of the 105th meridian* (Vol. 55). US Department of Commerce, National Oceanic and Atmospheric Administration.

Hope, A. S., & Schulze, R. E. (1982). Improved estimates of stormflow volume using the SCS curve number method. In V. P. Singh (Ed.), *Rainfall-runoff relationships* (pp. 419–431). Littleton: Water Resources Publications.

Liang, J., & Melching, C. S. (2015). Experimental evaluation of the effect of storm movement on peak discharge. *International Journal of Sediment Research*, *30*(2), 167–177. https://doi.org/10.1016/j.ijsrc.2015.03.004

Lobligeois, F., Andréassian, V., Perrin, C., Tabary, P., & Loumagne, C. (2014). When does higher spatial resolution rainfall information improve streamflow simulation? An evaluation using 3620 flood events. *Hydrology and Earth System Sciences*, *18*(2), 575–594. https://doi.org/10.5194/hess-18-575-2014

Midttømme, G., Pettersson, L. E., Holmqvist, E., Nøtsund, Ø., Hisdal, H., & Sivertsgård, R. (2011). Retningslinjer for flomberegninger (Guidelines for flood calculations). Retningslinjer no. 04/2011 (59 pp.). Retrieved from www.nve.no

Mizumura, K., & Ito, Y. (2011). Influence of moving rainstorms on overland flow of an open book type using kinematic wave. *Journal of Hydrologic Engineering*, *16*(11), 926–934. https://doi.org/10.1061/(ASCE)HE.1943-5584.0000398

Moretti, G., & Montanari, A. (2008). Inferring the flood frequency distribution for an ungauged basin using a spatially distributed rainfall-runoff model. *Hydrology and Earth System Sciences*, *12*(4), 1141–1152. https://doi.org/10.5194/hess-12-1141-2008

Nash, J. E., & Sutcliffe, J. V. (1970). River flow forecasting through conceptual models. Part I—A discussion of principles. *Journal of Hydrology*, *10*(3), 282–290. https://doi.org/10.1016/0022-1694(70)90255-6

Natural Resources Conservation Service (2007). *National engineering handbook: Chapter 16 Hydrographs*. Washington, DC: Natural Resources Conservation Service.

NERC (1975). *Flood studies report*. UK: Natural Environmental Research Council.

Niemi, T. J., Guillaume, J. H., Kokkonen, T., Hoang, T. M., & Seed, A. W. (2016). Role of spatial anisotropy in design storm generation: Experiment and interpretation. *Water Resources Research*, *52*, 69–89. https://doi.org/10.1002/2015WR017521

NSSP (1961). National severe storms project objectives and basic design. *Report no. 1*, U.S. Weather Bureau.

Rodriguez-Iturbe, I., & Mejía, J. M. (1974). On the transformation of point rainfall to areal rainfall. *Water Resources Research*, *10*(4), 729–735. https://doi.org/10.1029/WR010i004p00729

Scharffenberg, W. A., & Fleming, M. J. (2006). *Hydrologic modeling system HEC-HMS: User's manual*. US Army Corps of Engineers, Hydrologic Engineering Center.

Schulze, R. E. (1982). *The use of soil moisture budgeting to improve stormflow estimates by the SCS curve number method* (p. 63). Pietermaritzburg: University of Natal, Department of Agricultural Engineering.

Shen, Z., Chen, L., Liao, Q., Liu, R., & Hong, Q. (2012). Impact of spatial rainfall variability on hydrology and nonpoint source pollution modeling. *Journal of Hydrology*, *472*, 205–215.

Sigaroodi, S. K., & Chen, Q. (2016). Effects and consideration of storm movement in rainfall–runoff modelling at the basin scale. *Hydrology and Earth System Sciences*, *20*(12), 5063–5071. https://doi.org/10.5194/hess-20-5063-2016

Sivapalan, M., & Blöschl, G. (1998). Transformation of point rainfall to areal rainfall: Intensity-duration-frequency curves. *Journal of Hydrology*, *204*(1–4), 150–167. https://doi.org/10.1016/S0022-1694(97)00117-0

Smith, A., Sampson, C., & Bates, P. (2015). Regional flood frequency analysis at the global scale. *Water Resources Research*, *51*, 539–553. https://doi.org/10.1002/2014WR015814

USDA, Soil Conservation Service (1986). *Technical Release 55: Urban Hydrology for Small Watersheds* (2nd ed.).

Vaes, G., Willems, P., & Berlamont, J. (2005). Areal rainfall correction coefficients for small urban catchments. *Atmospheric Research*, *77*(1–4), 48–59. https://doi.org/10.1016/j.atmosres.2004.10.015

Veneziano, D., & Langousis, A. (2005). The areal reduction factor: A multifractal analysis. *Water Resources Research*, *41*, W07008. https://doi.org/10.1029/2004WR003765

Wright, D. B., Smith, J. A., & Baeck, M. L. (2014a). Critical examination of area reduction factors. *Journal of Hydrologic Engineering*, *19*(4), 769–776. https://doi.org/10.1061/(ASCE)HE.1943-5584.0000855

Wright, D. B., Smith, J. A., & Baeck, M. L. (2014b). Flood frequency analysis using radar rainfall fields and stochastic storm transposition. *Water Resources Research*, *50*, 1592–1615. https://doi.org/10.1002/2013WR014224

Wright, D. B., Smith, J. A., Villarini, G., & Baeck, M. L. (2013). Estimating the frequency of extreme rainfall using weather radar and stochastic storm transposition. *Journal of Hydrology*, *488*, 150–165. https://doi.org/10.1016/j.jhydrol.2013.03.003